Gap states in a-SiC from optical measurements and band structure models

2002 J. Phys.: Condens. Matter 14 1799

(http://iopscience.iop.org/0953-8984/14/8/309)

INSTITUTE OF PHYSICS PUBLISHING JOURNAL OF PHYSICS: CONDENSED MATTER

J. Phys.: Condens. Matter **14** (2002) 1799–1812 PII: S0953-8984(02)26233-5

Gap states in a-SiC from optical measurements and band structure models

V I Ivashchenko[1], V I Shevchenko[1], G V Rusakov[1], A S Klymenko[2], V M Popov[2], L A Ivashchenko[1] and E I Bogdanov[2]

[1] Institute of Problems of Material Science, NAS of Ukraine, Krzhyzhanovsky str. 3, 03142 Kyiv, Ukraine
[2] Center 'Microanalytics', Research Institute for Microdevices, Pivnichno-Syretskaya str. 3, 04136 Kyiv, Ukraine

E-mail: shev@materials.kiev.ua

Received 27 June 2001, in final form 7 November 2001
Published 15 February 2002
Online at stacks.iop.org/JPhysCM/14/1799

Abstract

Undoped and boron-doped a-$Si_{1-x}C_x$:H, for $x \approx 0.5$, films have been prepared by means of plasma-enhanced chemical-vapour deposition using methyltrichlorosilane. The optical absorption spectra of these films demonstrate three characteristic peaks at about 1.6, 2.0 and 2.5 eV consistent with other experimental measurements. To explain the observed peculiarities of the spectra, the atomic and electronic structures of a-SiC have been investigated using both molecular dynamics simulations based on an empirical potential and the recursion method. The results of the calculations show that five-coordinated (T_5) atoms (floating-bond atoms), anomalous four-coordinated (T_{4a}) sites (weak-bond atoms), three-coordinated (T_3) defects (dangling-bond atoms) and normal four-coordinated (T_{4n}) atoms which are nearest neighbours of T_3, T_{4a} or T_5 atoms give rise to three gap peaks. It was established that three peaks in the low-energy region of the optical absorption spectra are due to the electronic transitions: the valence band → the empty gap peak and two occupied gap peaks → the conduction band. Boron doping effects upon the optical spectra was not revealed.

1. Introduction

High-quality hydrogenated amorphous silicon carbide, a-SiC:H films have a wide interest in many photovoltaic and optoelectronic applications [1, 2]. It is well known that electrical transport properties of the films are strongly dependent on the defect states inside a bandgap (BG) [3, 4]. There are several types of defect which result in gap states (GS) appearing in an amorphous semiconductor material. We are interested in some of them: three-coordinated or dangling-bond (T_3) atoms, five-coordinated or floating-bond (T_5) atoms, strongly disordered

four-coordinated or weak-bond (T_{4a}) atoms and normal four-coordinated (T_{4n}) sites, which are the nearest neighbours of the T_3, T_{4a} or T_5 atoms. Other defects, such as micro-voids, are beyond of our consideration since they can be considered as a complex of the earlier-mentioned defects. Boron or other doping mixtures generate structural defects in amorphous semiconductor materials [5] therefore boron-doped a-SiC:H films were included in the scope of our investigations. The defects give rise to localized peaks in the BG and form the valence band (VB) and conduction band (CB) tails. If the latter causes a diffuseness of optical absorption spectra (OAS), defect levels modify these spectra in a low-energy range. Therefore, the low-energy thin structure in the OAS of amorphous semiconductor materials gives information about the GS distribution [8–13]. This information is very important, since most of the standard methods of determining GS are not applicable because of the low electrical conductivity of a-SiC:H films with a high carbon content (x_C).

Up to now there are only a few works devoted to the study of deep GS in a-SiC:H films by means of optical measurements [6–13]. The optical absorption measurements of undoped and doped μc–SiC:H PECVD films [6–8] have given some information about the influence of boron or nitrogen doping and defects on optical properties. Using photothermal deflection spectroscopy (PDS) and a constant photo-current method (CPM) Demichelis *et al* [9, 10] have detected silicon GS in the Si-rich alloys. The OAS of a-$Si_{1-x}C_x$:H films have been investigated by Bullot *et al* [11] and Skumanich, Frova and Amer [12]. On a basis of CPM measurements, Ligachov *et al* [13] have suggested the picture of the GS distribution in a-SiC:H films prepared by high-frequency sputtering. The main result of these investigations is the detection of several absorption coefficient peaks in the low energetic range, which points to the presence of localized states in the BG. From the optical measurements it follows that the peaks shift towards low energies as a carbon content decreases.

Konenkamp [14] revealed silicon GS in a light-activated charge-storage experiment on a-SiC:H films. The useful information concerning localized defect levels can be extracted from the photoluminiscence measurements of Engemann *et al* [15].

The atomic structure of a-SiC was studied by Finocchi *et al* [16], Kelires [17] and Tersoff [18] by theoretical methods. Molecular dynamics (MD) simulations based on fist-principles pseudopotential calculations [16] and classical Monte Carlo (MC) empirical simulations [17] have revealed that about 40% of the bonds formed by C are homonuclear. C-atoms give rise to both sp^2 and sp^3 sites. Si atoms give rise to strongly distorted diamond-like three-, four- and five-coordinated sites. Tersoff [18] has showed that carbon has only four-fold coordination. The density of states (DOS) of a-SiC has been investigated by Finocchi *et al* [16] and Kelires and Denteneer [19, 20] in the framework of an *ab initio* pseudopotential method using the local-density approximation (LDA) for the exchange- and correlation interaction between valence electrons. The obtained DOSs do not show a distinct gap because of underestimation of the BG in LDA-calculations [20], though the DOS of the 54-atom sample [16] has a distinct dip demonstrating the trend towards gap formation.

Chemical ordering in a-SiC has been studied in the framework of the free-energy model approach [21]. It was found that 89% of all bonds are Si–C bonds, with about 5% of each of the Si–Si and C–C bonds present [21].

So, the inspection of the problem of a-SiC and related materials enables us to conclude that, unlike the extensive theoretical study of the atomic and electronic structures of a-Si [22, 23], amorphous silicon carbide so far was studied incompletely.

In this paper we report the results of the OAS measurements of un-doped and boron-doped a-SiC:H films with a high carbon content prepared by plasma-enhanced chemical-vapour deposition (PECVD) from liquid methyltrichlorosilane (MTCS). To explain the peculiarities of the measured spectra and to establish the origin of localized states in the BG, the calculations

Table 1. Deposition parameters and some characteristics of a-SiC:H films. Notation: F_{MTCS}–MTCS expenditure; F_H, F_{BCl_3}—hydrogen and BCl_3 flow rates respectively; U_d–dc bias; T_s—substrate temperature; P_W—power of rf discharge; t—deposition time; d—film thickness; x_i–i atomic content; E_g—optic BG; σ_d—dark conductivity (x_O and x_{Cl} do not exceed 6 and 0.5 at.% respectively).

Sample	F_{MTCS} (sccm)	F_H (sccm)	F_{BCl_3} (sccm)	U_d (V)	T_s (°C)	P_W (W cm^{-3})
G01	0.011	17	0.000	−300	250	0.18
G02	0.011	60	0.000	−200	250	0.18
GP1	0.017	9	0.009	−30	230	0.44
GP2	0.015	4	0.009	−100	250	0.27

Sample	t (min)	d (nm)	x_C/x_{Si}	E_g (eV)	σ_d (S cm^{-1})
G01	120	600	0.92	2.42	0.5×10^{-6}
G02	120	480	1.11	2.60	1.3×10^{-6}
GP1	80	220	0.71	2.31	2.0×10^{-8}
GP2	40	135	0.97	2.43	0.6×10^{-8}

of the atomic and electronic structures of a-SiC were performed using both the MD simulation based on Tersoff's empirical potential and the recursion method (RM) of Haydock and Nex [24,25]. On the basis of the experimental and theoretical findings the possible explanation of the origin of GS in a-SiC was suggested.

2. Experimental details

The films discussed here were deposited in the (40.68 MHz) PECVD reactor at process pressures of 0.1–0.4 Torr from MTCS. The distance between two circular high-frequency electrodes of diameter 12.5 cm was kept constant at 2.5 cm. The liquid MTCS source was kept in the temperature range of 25–32 °C and the MTCS vapour was carried into the reaction chamber hydrogen gas. Hydrogen was supplied from a hydrogen accumulator, which represents the tank filled with $LaNi_5$ powder. The power was capacitively coupled to the plasma. The substrates used were crystalline silicon wafers, aluminium films, glass and quartz. The substrates were placed into the cylinder-like reaction chamber of stainless steel on the low electrode. An additional dc bias generated by a rf (5.27 MHz) generator was applied vertically to the substrates to create a negative potential at the substrate surface (U_d). Our deposition procedure gives average growth rates of ∼0.08 nm s^{-1}. To obtain boron-doped a-SiC:H films, the BCl_3 gas diluted in argon was added to a reactive gas mixture. The deposition regimes used to obtain a-SiC:H films and some characteristics of the films are summarized in table 1. The deposition conditions were chosen so that the formation of quality amorphous structure was enhanced [26].

The chemical composition of the films has been determined by means of an Auger spectrometer JUMP-10S, 'JEOL'. Dark conductivity measurements have been carried out at room temperature using a system for analysis of electro-physical parameters of semiconductor materials HP4061A, 'Hewlett-Packard'.

The transmission optical spectra of the films have been measured on a two-channel spectrometer SPECORD M400 'C.Zeiss' in the wavelength ranges of 300–900 nm and 200–900 nm for glass and quartz substrates, respectively. Obviously, the restricted apparatus possibilities do not allow narrow BG semiconductors, such as a-Si, a-Ge and Si-rich a-SiC:H

Table 2. Characteristics of the samples obtained from the 3C–SiC (D) and B1–SiC B1) melts at the same conditions by employing the modified potential. a_0—side of the cubic cell; R_{Si}—cut-off distance of Si–Si interactions; n_i—part of i-fold coordinated atoms; N_i—average coordination number of an atom i = Si, C; N_{i-j}—part of i–j (Si–Si, Si–C and C–C) bonds in the samples.

Sample	a_0 (nm)	R_{Si} (nm)	n_3 (%)	n_4 (%)	n_5 (%)	N_{Si}	N_C	N_{Si-Si} (%)	N_{Si-C} (%)	N_{C-C} (%)
D-64	0.8752	0.260	0.0	96.9	3.1	4.06	4.00	15.5	69.8	14.7
B1-64	0.8702	0.260	1.5	93.8	4.7	4.06	4.00	15.5	70.6	13.9
D-216	1.3086	0.260	2.0	92.0	6.0	4.12	3.96	15.4	71.5	13.1
B1-216	1.3056	0.250	1.8	90.3	7.9	4.12	4.00	16.4	68.8	14.8
D-512	1.7364	0.250	1.4	90.4	8.2	4.14	3.99	17.5	67.7	14.8
B1-512	1.7472	0.252	1.8	89.6	8.6	4.16	3.98	17.6	67.8	14.6

alloys, to be studied in the BG region, but are quite appropriate for carrying out the optical measurements of wide gap materials. From the transmission optical spectra, which represent interference fringes due to multiple reflections in the films, we have deduced the absorption coefficient α versus wavelength. Details, which concern a determination of this parameter from the spectra, have been reported elsewhere [27]. Film thicknesses have been determined with the help of a microprofiler ALPHA STEP-200 with an accuracy of about 1%. The value of the BG (E_g) has been evaluated according to Tauc's procedure [28] from an energetic dependency of the absorption coefficient.

3. Computational aspects

The atomic structure investigation of a-SiC has been carried out in the framework of MD simulations based on Tersoff's potential [18]. The sample, representing the diamond-like (D), or NaCl-like (B1) 64-, 216- or 512-atom cubic cell with periodic boundary conditions was heated at the constant zero pressure to 8000 K. Having reached 8000 K, the system was let free to evolve for ∼20 ps. The liquid obtained under such conditions is very similar to the one prepared by using a continuos-space MC method [17]. The melt was then quenched to 300 K with a cooling rate of 0.5×10^{13} K s^{-1}. The obtained sample was further equilibrated for 10 ps at 300 K. The comparison of the amorphous structures of the 64-, 216- and 512-atom samples originated from different melts shows that the atomic distribution in these samples is not very sensitive to the sample size and initial atomic configuration. This conclusion is confirmed by the data of table 2, where some characteristics of a-SiC samples are summarized.

Special attention was paid to matching some parameters of Tersoff's potential for 3C–SiC [18] to obtain the amorphous network with a maximum amount of T_4 atoms. Though there are a few a-SiC investigations, in which T_3 carbon atoms (graphite-like coordinated atoms) were found, recent works [21, 29, 30] demonstrate that a-SiC has preferably four-fold coordination and the high extent of chemical ordering (predominance of Si–C bonds) (the review on this problem is performed in [16, 20, 21]). Therefore, in the scheme [18], the C-potential was exchanged by the new Tersoff [31] potential, which describes correctly defects in diamond. However, the application of this scheme turned out to lead to the strongly disordered structures only having about 40% silicon T_4 atoms. Consequently, this approach is unable to provide the appropriate results. Keeping in mind that in Tersoff's formalism, the cutoff parameters R and S were chosen somewhat arbitrarily and were not systematically optimized [32], we have carried out several calculations with various R and S parameters. It was established that the optimal amorphous structure having as many as possible T_4 atoms can

be reached at $R = 0.25$ nm, $S = 0.27$ nm. For comparison, we have calculated a-SiC using the C-potential determined from graphite [33] and which has been used in MC simulations [17]. The obtained sample contained a considerable portion of T_3 graphite-like carbon atoms. Since such atoms are present in an appreciable amount in the carbon-rich alloys [34], we deduce that the modified scheme of Tersoff is more suitable for describing the atomic characteristics of a–$Si_{1-x}C_x$ alloys, for $x \leqslant 0.5$. More detailed information supporting this conclusion can be also found elsewhere [18].

The DOS of the samples was calculated by the RM of Haydock and Nex [24, 25], a deconvolution procedure and using eigenvalues of the tight-binding matrix in 35 k-points of the irredusible segment of the Brillouin zone (BZ) of the cubic lattice with a unit cell of 64 atoms. In the RM calculations, the initial cell was spread to a large cluster of 4096 atoms conformable to periodic conditions. The DOS of silicon carbide was accurately constructed using the approach of Nex [25], retaining 54 levels of recursion coefficients [35]. The comparison of the DOSs obtained in the framework of the three mentioned methods has showed that these procedures give similar results.

A $sp^3s^\star$ interpolation scheme [36] was used to reproduce the energy bands of Si, C and 3C–SiC. We have taken tight-binding parameters for these materials from [34] as the input data. Furthermore, they have been updated by means of fitting the tight binding energy bands to eigenvalues in eight energetic bands for c-Si [37], 3C–SiC [34] and diamond [38]. The fitting enabled us to reproduce the initial bands with high accuracy. For comparison, the energetic interval Γ–$\Sigma_{\min}$ in 3C–SiC is 7.2, 5.1 and 3.7 eV according to experiment [34], our data and Robertson's calculation [34], respectively. Our scheme gives the C and Si dangling bond states in 3C–SiC at about 0.4 and 2.1 eV (above the VB top), which is very close to our previous findings (0.5 and 1.98 eV) [35] and the recent data [39] (0.38 and 2.15 eV). A single vacancy in c-Si and diamond gives rise to gap levels at 0.3 and 1.55 eV, correspondingly. The parameters were changed depending on bond lengths (R) as R^{-2}, according to the Harrison rule [40].

The energy bands of Si, C and 3C–SiC were aligned following the procedure of the superposition of the Si K-, Si L- and C K–emission bands in a-$Si_{1-x}C_x$:H alloys [41]. Also taking into account recommendations for this problem [34], we have chosen the band limits as follows. The zero of energy of the system is at the top of the VB of c-Si; so, the gap in c-Si lies at 0.0–1.15 eV, that of 3C–SiC between -1.2 and 1.2 eV and that of diamond between -2.55 and 2.95 eV.

4. Results and discussion

The chemical composition and some characteristics of the films are reported in table 1. All the samples were prepared in starving plasma conditions, when the MTCS expenditure is small. Such samples with a large optic gap possess a comparably high dark conductivity, which means that the films have a small microcrystalline fraction. The high oxygen concentration is also one of the features of microcrystallinity. It is known [42] that oxygen is a common contaminant of microcrystalline films. Much of it is probably chemically bonded to the grain boundaries. The boron-doped films demonstrate a low dark conductivity compared with the un-doped ones, which implies that the GP1 and GP2 samples are less microcrystalline than the G01 and G02 samples. Such a situation is supposed to be due to a hydrogen dilution of MTCS, which was higher in preparing the latter samples than at the deposition of the boron-doped films. The hydrogen dilution of reactive gases leads to the passivation of dangling or weak bonds and promotes the appearance of crystalline islets in an amorphous tissue [6, 7].

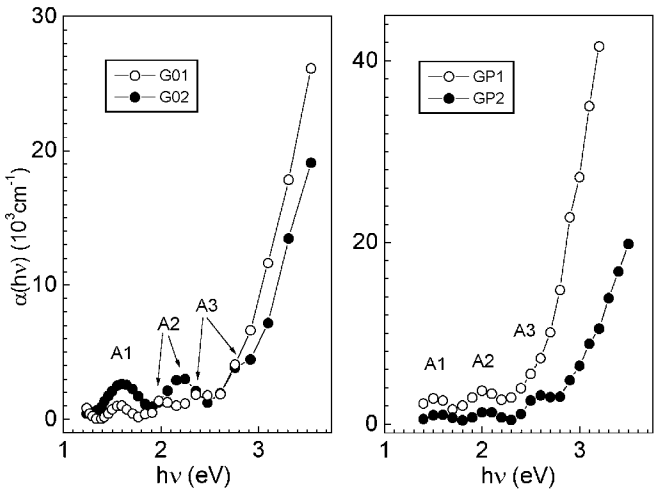

Figure 1. Absorption coefficient as a function of energy of undoped and boron-doped a-SiC:H films.

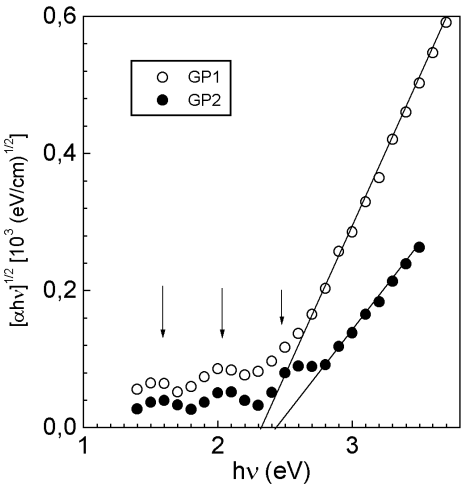

Figure 2. Tauc plots of the boron-doped films.

In figure 1 we show the absorption coefficient curves of un-doped and boron-doped a-SiC:H films. Figure 2 shows Tauc plots for the boron-doped samples. There are three peaks located at about 1.4–1.6 eV (A1), 2.0–2.2 eV (A2) and 2.5–2.8 eV (A3) in the OAS. The optical BG determined from Tauc plots (figure 2) widens with increasing the carbon content in all the samples (table 1). Our findings are very close to the CPM and PDS results for a-SiC:H films [11, 13]. The comparison of the left and right plots in figure 1 does not give any information about the influence of boron on the optical spectra. Because of this circumstance we deduce that the boron admixture alters $\alpha(h\nu)$ considerably less than structural defects. Skumanich *et al* [12] and Ligachov *et al* [13] have stressed that the low-energy peaks in the OAS should be attributed to GS originating from structural defects. Since the absorption coefficient reported in figure 1, as deduced from transmittance measurements, cannot give the

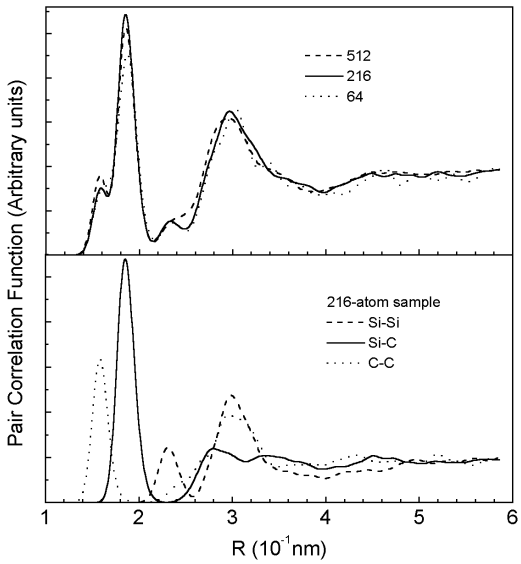

Figure 3. Total (upper panel) and partial (lower panel) PCF in D-64, D-0.516 and B-512 samples.

unambiguous information concerning localized gap levels, we appeal to the results [9–13]. From these results it follows that all the A1, A2 and A3 peaks are shown only in the spectra of a-SiC:H films with a high carbon content. The peaks shift toward low energies as x_C decreases. In the Si-rich alloys the A2 and A3 peaks are absent, and the A1 peak is now located at about 1.2–1.4 eV.

Figure 3 displays the computed total pair correlation functions (PCF) $g(r)$, normalized so $g(\infty) = 1$, for the B-512, D-216 and D-64 alloys (upper panel) and the partial PCFs $g_{i-j}(r)$ (i, j = C, Si), for the D-216 sample (bottom panel). From figure 3 one can see that the pictures of the atomic distribution in all the samples are similar which means that the atomic structure of the samples is small sensitive to their sizes. The partial PCFs show that the g_{C-C} has an intense first peak at 0.157 nm to be compared with the nearest-neighbour distance in diamond (0.155 nm). Like to the results of Finocchi *et al* [16] and Tersoff [18] we found one secondary maximum at 0.296 nm corresponding to the C–Si–C configuration and a shoulder at ∼0.276 nm associated with C–C–C correlation. The partial coordination number of C n_{C-C}, as computed from the integral of g_{C-C} up to its first minimum, is 1.16. The C–Si PCF has a first peak at 0.186 nm and a second peak at 0.278 nm, with $n_{Si-C} = 2.8$. Thus, each C atom has on an average about 3.96 neighbours (due to several T_3-atoms). The g_{Si-Si} curve has a broad range of neighbouring distances. The sharp dip in the Si–Si PCF at around 0.26 nm (as in [18] near 0.28 nm) is somewhat an artefact of the cutoff of the potential [33]. We have defined that n_{Si-Si} was constant and equal to about 1.28 by varying the cutoff distance R_{Si-Si} in the range 0.25–0.26 nm. It means that a silicon atom is surrounded on an average by 4.12 neighbours, which is due to 13 stable T_5 silicon atoms which have been found to be present in the D-216 sample.

In figure 4 we report the bond-angle distribution $g(\theta)$ in the D-64 sample, where θ denotes the angle between two vectors that join a central particle with two neighbours at a distance less than the first minimum in the corresponding $g(r)$. All peaks of the distribution are shifted toward small angles relative to the ideal diamond-like dihedral angle of 109.47°. The mean bond angle for carbon and silicon is 109.3° and 108.26° respectively, and the total mean bond angle is equal to 108.77°. The results presented in figure 4 and the data on bond-length deviation show that silicon atoms are distributed more randomly than carbon ones.

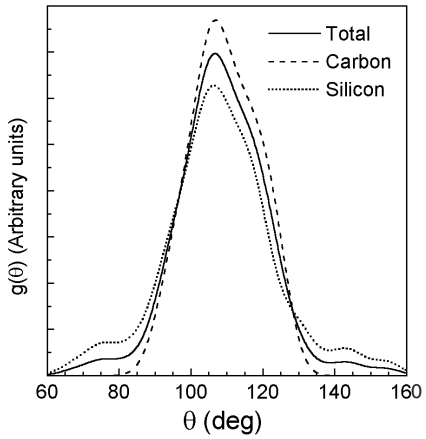

Figure 4. Total and partial bond-angle distributions in the D-64 sample.

Our samples differ from other models [16, 17] first of all owing to the considerable predominance of Si–C correlations and a little of T_3-atoms. Our structures are more similar to the cubic silicon carbide 3C–SiC than other ones [16,17]. But, on the other hand, they are also close to the a-Si model [22]. The samples are characterized by the availability of stable T_5-atoms, which are present in the models in much greater magnitude than T_3-atoms. The picture of a-SiC, which emerges from our structural analysis is consistent with the model of a-Si of Pantelides [43,44]. It was shown [43,44] that the electron paramagnetic resonance active centre in a-Si can be identified as T_5 atoms and corresponds to the floating-bond-type defect. The samples also contain atoms located inside strongly deformed tetrahedrons, and for this reason can be characterized as distorted tetrahedral sites. These atoms have several weak bonds, which give rise to GS. A weak-bond-type defect involves particles at distances intermediate between the first and second peak of $g(r)$ and which have dihedral bond-angles belonging to the tails of $g(\theta)$ (figure 4). So, our samples consist of slightly distorted tetrahedral sites (T_4), T_3, T_5 sites and strongly distorted tetrahedral sites, T_{4a}. We also single out four-coordinated atoms (T_{4n}) which are the neighbours of abnormally coordinated atoms. To anticipate a little, all these atoms, with the exception of T_4 sites, make a contribution to GS.

The total and local DOSs of different samples are presented in figures 5 and 6. The electronic spectrum of the D-64 sample in the BG range is shown in figure 7. From figure 5 we see that the electronic spectra coincide well over the entire energetic range with the exception of the VB bottom. The latter is explained by the fact that the RM can give spurious DOS peaks at spectrum edges, especially in small samples [24, 25]. The formation of a semiconducting gap is observed in all the spectra in agreement with experiment. The determination of the BG in a-SiC turned out to be not a simple task due to smearing the DOS at band edges caused by the specificity of our computer procedures. However, a superposition of the total DOSs of a-SiC and 3C–SiC allowed us to evaluate the gap position. Herewith, we have taken into consideration the tendency in varying the DOS in the BG range on going from the strongly disordered alloys (B-512, D-216) to the small disordered sample (D-64). The gap was found to range from about -1.4 to 1.05 eV and to be equal to about 2.45 ± 0.1 eV. In this range three defect-induced peaks P1, P2, P3 were observed at -1.2, -0.4 and 0.35 eV, respectively. One of them, P1, can be identified as a resonance peak due to its localization at the VB tail. Evidence of the availability of three peaks inside the BG is strongly supported by the recursion DOS. Unlike the Gaussian broadening DOS, the recursion one unambiguously shows three

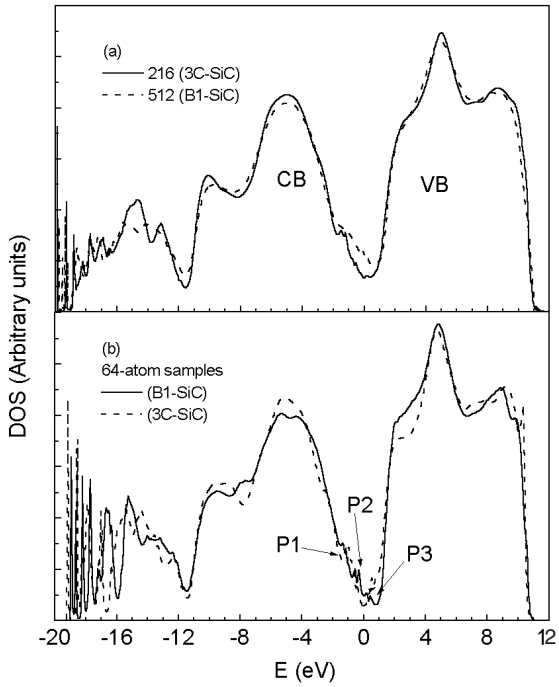

Figure 5. Total densities of states in the D-64, B-64, D-216, B-512 samples.

mentioned peaks in the BG range (figure 7). However, it should be noted that the peak positions are rather determined approximately due to the uncertainty in finding the BG range.

The local DOSs presented in figure 6 enable one to establish the origin of the BG peaks. The P1 peak originates from the states of the silicon T_{4a}, T_5 atoms (Si–Si_3C and Si–Si_4C configurations) and, to a small extent, carbon T_4 atoms (C–SiC_3 configuration). Weak- and dangling-bond carbon atoms in the C–Si_4 and C–SiC_2 configuration, respectively, and weak- and floating-bond silicon atoms in the Si–SiC_3 and Si–SiC_4 configuration, respectively, cause the P2 maximum. The P3 peak is mostly attributed to silicon T_5 and T_{4a} atoms (Si–Si_4C and Si–SiC_3 configurations). Silicon dangling-bond states related to T_3-atoms in the Si–C_3 configuration determine the CB tail (figure 6(b)). From figures 6(b), (d) one can see that dangling-bond GS are localized more strongly than other defect states. Carbon-induced GS turned out to arise only due to disordering Si–C bonds. No deformed C–C bonds giving rise to GS have been revealed. Naturally, the peak positions deviate inconsiderably from the mentioned positions (± 0.04 eV) depending on the surrounding. As far as T_5-atoms are concerned, an extra floating bond leads to an unpaired electron spin on the neighbouring atoms. Our results indicate that this unpaired electron can be somewhat delocalized and is able to resonate between three or four neighbours [45], or can be localized, in which case the floating bond consists of a single dominant site involving an unpaired electron spin with one secondary atom [46].

We have compared our findings with the experimental results on deep-lying defects in a-SiC:H alloys. From a charge-storage experiment, Konenkamp [14] have found the negatively charged Si dangling-bond level at 1.15 eV down the CB edge. According to our results, this level can be identified with the peak P2 located at about 1.45 eV down the CB edge. Two luminescence peaks at 1.3 eV and 1.8 eV detected in a-$Si_{1-x}C_x$:H, $x \approx 0.5$ films [15] can be

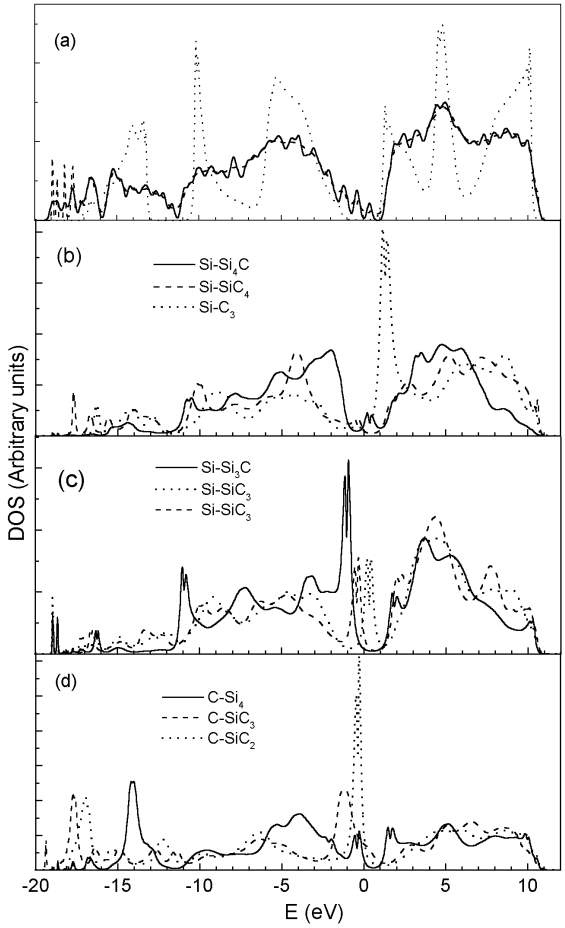

Figure 6. Total DOS determined by the RM for 3C–SiC (dotted curve), a-SiC (dashed curve) and constructed from eigenvalues for a-SiC (full curve) (a). Recursion local DOS related to silicon atoms (b), (c) and carbon atoms (d) sited in different surroundings.

interpreted as the electronic transitions from CB to P2 (1.45 eV) and from P3 to VB (1.75 eV). The shoulder at 1.4 eV and the smeared maximum at about 2.2 eV in the photoluminescence spectrum of the a-$Si_{0.43}C_{0.57}$:H alloy [15] were suggested to be formed as a result of the CB→P2 (1.45 eV) and CB→P1 (2.25 eV) transitions.

Figure 5 illustrates that the energetic position of the peaks remains approximately constant for all samples. This circumstance makes it possible to predict the DOS of an amorphous sample with a small number of defects. Such a DOS model is shown in figure 8. It consists of the parabolic VB and CB, separated by an energy gap of 2.45 eV and contains three Gaussian smoothed GS peaks. The VB and CB edges of the DOS model are smoothed by a 0.1 eV Gaussian. The zero of energy is superposed with the Fermi level that is located between the peaks P2 and P3. The DOS model has the same bandwidths and capacity as the recursion DOS. From figure 8 one can see that the DOS model agrees well with the eigenvalues-based DOS, though there is one essential difference. That is the peak widths in the latter spectrum are appreciably larger than those in the DOS model, which implies that the latter electronic spectrum belongs to the more perfect amorphous material.

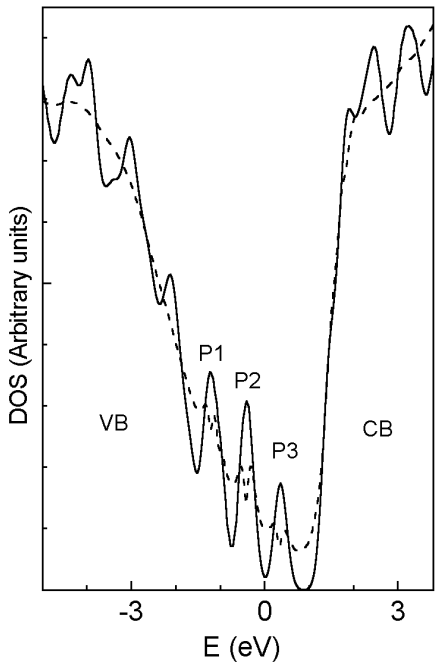

Figure 7. Total DOS in the BG range calculated by RM (dashed curve) and from eigenvalues (full curve) for the D-64 sample.

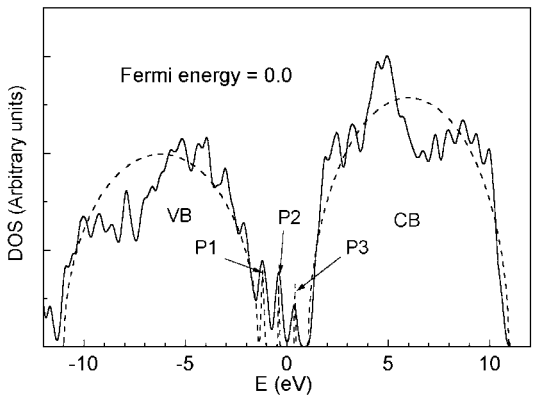

Figure 8. Eigenvalues based DOS (D-64, full curve) and DOS model (dashed curve).

Using the band structure model for a-SiC alloy, we have calculated the absorption optical coefficient from the expression

$$\alpha(\nu) = \frac{A}{h\nu} \int_{-\infty}^{\infty} N_{\mathrm{i}}(E)\, f_{\mathrm{FD}}(E)\, [1 - f_{\mathrm{FD}}(E + h\nu)]\, N_{\mathrm{f}}(E + h\nu)\, \mathrm{d}E \tag{1}$$

where A is a constant representing an optical matrix element, $N_{\mathrm{i}}(E)$ and $N_{\mathrm{f}}(E + h\nu)$ are the initial and final DOS, $h\nu$ is photon energy and $f_{\mathrm{FD}}(E)$ is the Fermi–Dirac distribution. In calculating α from (1), we have taken into account the following transitions: VB $\rightarrow$ CB, VB $\rightarrow$ P3, P1 $\rightarrow$ CB, P2 $\rightarrow$ CB. The constant A was the same for all these contributions [47].

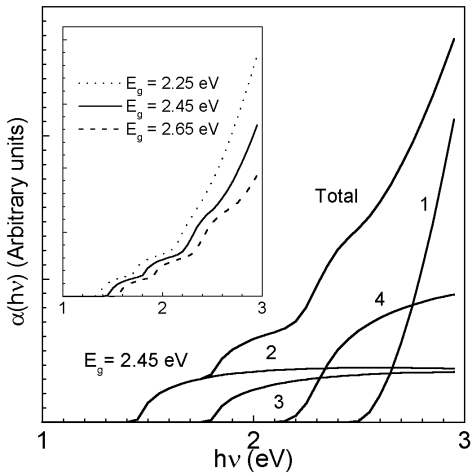

Figure 9. Calculated absorption optical coefficients for a-SiC. Partial contributions: 1–VB→CB, 2–P2→CB, 3–VB→P3 and 4–P1→CB. In the inset, absorption coefficients calculated from the band structure model (figure 8) for different gap widths.

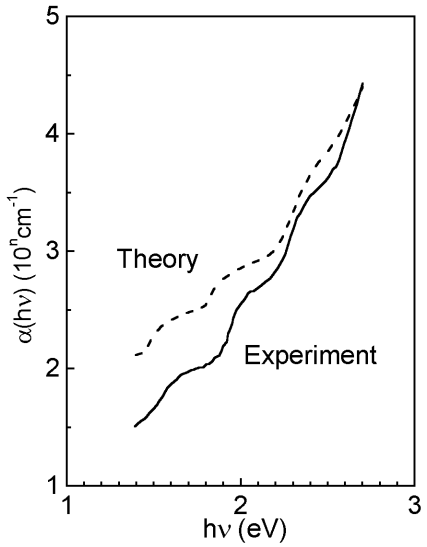

Figure 10. Results of a superposition of the measured [13] ($E_g = 2.44$, full curve) and calculated ($E_g = 2.45$, dashed curve) absorption optical coefficients.

The calculated absorption coefficient is demonstrated in figure 9. In figure 10 a superposition of the theoretical and experimental absorption coefficients is performed. Using the data of figures 9, 10 it is easy to identify the origin of the optical peaks. In particular, the A1 peak originates from the electronic transition P2→CB (curve 2), the A2 from VB→P3 (curve 3) and the A3 from P1→CB (curve 4). The high-energy region of the spectrum is formed by the electronic transitions VB→CB. The inset in figure 9 shows that on going from the wide gap samples to the narrow gap alloys the peaks shift towards low energies, herewith, the A3 peak disappears owing to dissolving the P3 states in the VB tail.

Finally, we have to stress that the findings based on the band structure models have the semi-quantity character since many factors were not taken into account, in particular, the influence of hydrogen and microcrystallinity on film characteristics. In weakly hydrogenated silicon carbide films GS are always shown more distinctly than in the strongly hydrogenated samples because a little of the hydrogen cannot be sufficient to make passivation of all disturbed bonds. The predominance of silicon un-saturated bonds in the films is explained by a fact that the C–H bond is stronger than the Si–H bond, which leads to the preferential attachment of H to C. In the case of the microcrystalline films, when the absorption coefficient is derived from a superposition of the absorption coefficients for amorphous, crystalline and grain boundary regions [48], one can expect strengthening of the A3 peak owing to the direct transitions inside 3C–SiC islets with $E_g = 2.4$ eV. Our preliminary investigations have shown that it is the 3C–SiC crystallites that are present in μc-$Si_{1-x}C_x$:H films, for $x \sim 0.5$. However, since the crystalline fraction in the films is small, we believe the theoretical findings on a-SiC to be appropriative in explaining the optical properties of μc-SiC:H alloys.

5. Conclusions

We have studied the OAS of un-doped and boron-doped a-SiC:H films prepared by PECVD from MTCS. The spectra show three peaks at about 1.6, 2.0 and 2.5 eV. The boron incorporation into the films does not lead to any appreciable changes in the absorption spectra. The MD empirical simulations—recursion calculations of a-SiC enabled the origin of three gap peaks to be established. GS were found to be caused by five-fold coordinated atoms (floating bonds), abnormally four-fold coordinated sites (weak bonds), three-coordinated defects (dangling bonds) and normal four-coordinated atoms, which are nearest neighbours of abnormal-coordinated atoms (weak bonds). The absorption peaks in the low-energy region are due to the electronic transitions between two occupied gap peaks, one empty gap peak, the VB and CB tails. The agreement found between the calculated and experimental characteristics supports our band structure model of a-SiC.

References

[1] Bullot J and Schmidt M P 1987 *Phys. Status Solidi* **143** 34
[2] Hamakawa Y 1998 *Renew. Energy* **15** 22
[3] Hamakawa Y (ed) 1983 *Amorphous Semiconductors* (Tokyo: OHM)
[4] Joannopoulos J D and Lucovsky G (ed) 1984 *The Physics of Hydrogenated Amorphous Silicon* vols 1 and 2 (Berlin: Springer)
[5] Ristein J and Weiser G 1985 *Sol. Energy Mater.* **12** 221
[6] Demichelis F, Pirri C F and Tresso E 1992 *J. Appl. Phys.* **72** 1327
[7] Demichelis F, Grovini G, Pirri C F, Tresso E, Fanciulli M, Pjesarkiewicz T and Stapinski T 1994 *Semicond. Sci. Technol.* **9** 1543
[8] Hadjadj A *et al* 1998 *J. Appl. Phys.* **83** 830
[9] Demichelis F *et al* 1993 *J. Non-Cryst. Sol.* **164–6** 10
[10] Demichelis F, Giorgis F, Pirri C F, Tresso E, Amato G and Coscia U 1995 *Physica* B **205** 169
[11] Bullot J, Gautheir M, Schmidt M P and Catherine Y 1985 *Solid State Commun.* **54** 107
[12] Skumanich A, Frova A and Amer N M 1985 *Solid State Commun.* **54** 597
[13] Ligachov V A, Svikrova N N, Filikov V A and Vasiljeva N D 1996 *Phys. Techn. Semicond.* **30** 1601
[14] Konenkamp R 1987 *Phys. Rev.* B **36** 2938
[15] Engemann D, Fischer R and Knecht J 1978 *Appl. Phys. Lett.* **32** 567
[16] Finocchi F, Galli G, Parrinello M and Bertoni C M 1992 *Phys. Rev. Lett.* **68** 3044
[17] Kelires P C 1992 *Phys. Rev.* B **46** 10 048
[18] Tersoff J 1994 *Phys. Rev.* B **49** 16 349
[19] Kelires P C and Denteneer P J N 1993 *Solid State Commun.* **87** 851

[20] Kelires P C and Denteneer P J H 1998 *J. Non-Cryst. Solids* **231** 200
[21] Efstathiadis H, Yin Z and Smith F W 1992 *Phys. Rev.* B **46** 13 119
[22] Stich I, Car R and Parrinello M 1991 *Phys. Rev.* B **44** 11 092
[23] Peressi M, Fornari M, De Girodcolli S, De Santis L and Baldereschi A 2000 *Phil. Mag.* **80** 515
[24] Haydock R, Heine V and Kelly M J 1972 *J. Phys. C: Solid State Phys.* **5** 2845
[25] Nex C M M 1984 *Comput. Phys. Commun.* **34** 101
[26] Ivashchenko L A, Rusakov G V and Ivashchenko V I 1999 *Appl. Surf. Sci.* **138–9** 444
[27] Bennouna A, Loaziz Y and Idrissi M A 1992 *Thin Solid Films* **213** 55
[28] Tauc J and Menth A 1972 *J. Non-Cryst. Solids* **8–10** 569
[29] Efstathiadis H, Yin Z and Smith F W 1992 *Phys. Rev.* B **46** 13 119
[30] Evangelisti F 1993 *J. Non.-Cryst. Solids* **164–6** 1009
[31] Tersoff J 1990 *Phys. Rev.* B **64** 1757
[32] Tersoff J 1988 *Phys. Rev.* B **38** 9902
[33] Tersoff J 1989 *Phys. Rev.* B **39** 5566
[34] Robertson J 1992 *Phil. Mag.* **66** 615
[35] Ivashchenko V I, Shevchenko V I, Ivashchenko L A and Rusakov G V 1999 *J. Phys.: Condens. Matter* **11** 3265
[36] Vogl P, Hjalmarson H J and Dow J D 1983 *J. Phys. Chem. Solids* **44** 365
[37] Herman F, Kortum R L and Kuglin C D 1967 *Int. J. Quant. Chem.* **1** 533
[38] Zunger A and Freeman A 1977 *Phys. Rev.* B **15** 5049
[39] Gubiotti G, Kucherenko Yu, Yaresko A, Perlov A and Antonov V 2000 *J. Phys.: Condens. Matter* **12** 3369
[40] Harrison W A 1980 *Electronic Structure and the Properties of Solids* (San Francisco: Freeman)
[41] Wiech G, Langer H, Lepa U and Simunek A 1993 *J. Non-Cryst. Solids* **164–6** 1023
[42] Veprek S, Iqbal Z, Kuhne R O, Capezzuto P, Sarott F A and Ginzewski J L 1983 *J. Phys. C: Solid State Phys.* **16** 6241
[43] Pantelides S T 1986 *Phys. Rev. Lett.* **57** 2979
[44] Pantelides S T 1987 *Phys. Rev. Lett.* **58** 1344
[45] Biswas R, Wang C Z, Chan C T, Ho K M and Soukoulis C M 1989 *Phys. Rev. Lett.* **63** 1491
[46] Stathis H I 1989 *Phys. Rev.* B **40** 1232
[47] Amato G, Goirgis G and Spagnolo R 1992 *J. Appl. Phys.* **71** 3479
[48] Dichl F, Scheib M, Schroder B and Oecgsner H 1998 *J. Non-Cryst. Solids* **230** 973